

Wind load estimation of super-tall buildings based on response data

Lun-hai Zhi^{*1}, Bo Chen^{2a} and Ming-xin Fang^{1b}

¹School of Civil Engineering and Architecture, Wuhan University of Technology, Wuhan 430070, China

²Key Laboratory of Roadway Bridge and Structural Engineering, Wuhan University of Technology,
Wuhan 430070, China

(Received February 7, 2015, Revised November 4, 2015, Accepted November 6, 2015)

Abstract. Modern super-tall buildings are more sensitive to strong winds. The evaluation of wind loads for the design of these buildings is of primary importance. A direct monitoring of wind forces acting on super-tall structures is quite difficult to be realized. Indirect measurements interpreted by inverse techniques are therefore favourable since dynamic response measurements are easier to be carried out. To this end, a Kalman filtering based inverse approach is developed in this study so as to estimate the wind loads on super-tall buildings based on limited structural responses. The optimum solution of Kalman filter gain by solving the Riccati equation is used to update the identification accuracy of external loads. The feasibility of the developed estimation method is investigated through the wind tunnel test of a typical super-tall building by using a Synchronous Multi-Pressure Scanning System. The effects of crucial factors such as the type of wind-induced response, the covariance matrix of noise, errors of structural modal parameters and levels of noise involved in the measurements on the wind load estimations are examined through detailed parametric study. The effects of the number of vibration modes on the identification quality are studied and discussed in detail. The made observations indicate that the proposed inverse approach is an effective tool for predicting the wind loads on super-tall buildings.

Keywords: inverse technique; wind load; super-tall building; continuous-time Kalman filter; wind-induced response; wind tunnel test

1. Introduction

Super-tall buildings ('super-tall' is defined as a building over 300 m in height by the Council on Tall Buildings and Urban Habitat) have been constructed commonly with light weight and high strength materials in recent years; tend to be more flexible and lightly damped than those built in the past. Therefore, tall buildings are more sensitive to strong winds and other dynamic excitations. It is thus required to investigate the wind effects on such wind-sensitive structures (Ha 2013, Chakraborty *et al.* 2014). At present, wind tunnel testing is a relatively mature technique to

*Corresponding author, Associate Professor, E-mail: zhilunhai1979@163.com

^aProfessor, E-mail: cbsteven@163.com

^bPh.D. Student, E-mail: fm126@163.com

pre-estimate the design wind loads and wind induced responses of civil engineering structures. However, it is generally difficult to reproduce the exact field conditions such as incident turbulence and terrain characteristics in wind tunnel tests so as to result in uncertainties in the estimation of wind loads. Field measurement or monitoring is regarded as the most reliable way in the investigation of wind effects on prototype buildings and structures. Nevertheless, it is very difficult or not feasible to measure the wind loads applied on an existing building directly. Hence, indirect measurement techniques, which are also known as wind load estimation techniques are sought as an alternative approach.

The external load identification from the measured dynamic responses of a structure is one of typical inverse problems. Many alternative methods have been presented and developed (Stevens 1987, Sanchez and Benaroya 2014). Wu and Law (2010) grouped the forces identification methods into three categories: Deterministic methods, Stochastic methods, and Artificial intelligence based methods. Deterministic methods require a mathematic model to represent the system and can be sub-divided into the frequency domain methods and the time domain methods. Stochastic methods are based on a stochastic system model and provide a statistical relationship between the external load and the structural response. Artificial intelligence based methods require a learning process to establish the relationship between the input and output. Each of these methods has its strengths and drawbacks. For example, the frequency domain methods can provide satisfactory load estimation quality for linear time-invariant systems, while the time domain methods are applicable to solve time variant problems. The Stochastic methods treat the structure-load interaction problem with uncertainty in which the identified results are supplemented with their statistical information. More detailed information on these methods can be found in previous studies.

Several methods have been developed recently to estimate the wind forces on structures using wind-induced responses. Chen and Li (2001) proposed a time domain identification method for inverting wind input process when structural parameters are unknown. Nagashima *et al.* (2001) suggested a force identification method for estimating the wind loads acting on a 36-story building with a hybrid mass damper system using observed acceleration responses. Kang and Lo (2002) presented an inverse matrix procedure based on discretized governing equations to estimate the strength of wind drags on an elevated tower and the magnitude of the vibration of the ground on which the tower stands. Law *et al.* (2005) proposed a method to estimate the longitudinal time-varying wind loads on a 50m guyed mast using measured structural displacement responses. Hwang *et al.* (2009, 2011) presented a practical inverse approach for estimating wind modal loads using limited measured responses based on the Kalman filter, and applied the method to identify the wind loads acting on a 210-m chimney. However, the literature review reveals that an indirect estimation for the wind loads acting on super-tall buildings have rarely been carried out in the past. It is necessary to conduct such a study, since the estimated wind loads using measured structural responses are valuable for the wind-resistant design of modern super-tall buildings.

An effective inverse method is developed based on the continuous-time Kalman filter in this study. This method extends an existing input and state estimation filter to the identification of real wind loads on each measurement layer on a super-tall building based on limited structural responses (Kalman and Bucy 1961, Hwang *et al.* 2009, 2011). An optimum solution of Kalman filter gain by solving the Riccati equation is employed to improve the identification accuracy. The proposed method is applied to the estimation of wind loads on a typical super-tall building based on wind tunnel test results. The wind loads on the super-tall building are first determined in a wind tunnel test by using the pressure scanning technique. The direct wind-induced responses of the structural system are evaluated based on structural dynamic analysis. The inverse algorithm then

uses the selected responses (acceleration or displacement responses) to estimate the corresponding wind forces.

The accuracy of the external load estimation technique is examined through the comparison between the estimated and exact input forces. Furthermore, the effects of several factors such as the type of wind-induced response, the covariance matrix of noise, errors of structural modal parameters, levels of noise in the measured responses and the number of vibration modes on the wind load estimation are evaluated and discussed in detail. The main aim of this study is to verify the inverse method as an effective tool for predicting the wind loads on super-tall buildings.

2. Inverse analysis procedure

2.1 Estimation of modal wind-induced responses

The equation of motion of a super-tall building with “ n ” floors subjected to random wind loads can be commonly written as follows

$$\mathbf{M}\ddot{\mathbf{y}} + \mathbf{C}\dot{\mathbf{y}} + \mathbf{K}\mathbf{y} = \mathbf{F} \quad (1)$$

Where \mathbf{M} denotes $n \times n$ mass matrix, \mathbf{C} denotes the $n \times n$ damping matrix and \mathbf{K} denotes the $n \times n$ stiffness matrix, respectively. \mathbf{y} , $\dot{\mathbf{y}}$ and $\ddot{\mathbf{y}}$ are displacement vector, velocity vector and acceleration vector, respectively. \mathbf{F} is the time history vector of the fluctuating wind load, which is generally treated as a stationary random process.

If the complete responses of a structure are known, the wind loads acting on the building can be easily computed by Eq. (1). However, the measurement of complete responses for all degrees of freedom is infeasible in practice and only displacement or acceleration responses are generally measured or available. The estimation of complete responses from limited responses is required. In this study, the continuous-time Kalman filter is employed to estimate the unknown responses. The Kalman filter is classically applied to the problem of estimating unknown states from noisy measurements. Owing to its relative simplicity and robust nature, the Kalman filter has been widely used to obtain estimates of the state variables in practice (Ma *et al.* 2003, Hwang *et al.* 2009, 2011, Lourens *et al.* 2012, Azam *et al.* 2015, Naets *et al.* 2015). The detailed description of the Kalman filter can be found from Kalman and Bucy (1961).

Assuming that the system matrices (mass and stiffness) of a super-tall structure are fully known, which can be obtained by the finite element method (FEM). If accelerations for all degrees of freedom are measured only, the structural acceleration vector can be expressed by the following formula

$$\ddot{\mathbf{y}}_{n \times 1} = \Phi_{n \times n} \ddot{\mathbf{U}}_{n \times 1} \quad (2)$$

where $\Phi_{n \times n}$ is the $n \times n$ mode shape matrix; n is the total node number of a structure. $\ddot{\mathbf{U}}_{n \times 1}$ is the modal acceleration response vector.

Owing to the limitation of the number of sensors and identified mode shapes, a reduced-order representation of the measured acceleration responses is approximately given by

$$\ddot{\mathbf{y}}_{p \times 1} = \Phi_{p \times q} \ddot{\mathbf{U}}_{q \times 1} \quad (1 \leq p \leq n, 1 \leq q \leq n) \quad (3)$$

where $\Phi_{p \times q}$ is the $p \times q$ mode shape matrix corresponding to the highest q vibration mode.

Using the pseudo-inverse of the modal transformation matrix $\Phi_{p \times q}$, the modal acceleration responses can be approximately calculated from the measured acceleration responses as follows

$$\begin{cases} \hat{U}_{q \times 1} = (\Phi_{p \times q})^+ \ddot{y}_{p \times 1} \\ \hat{U}_{q \times 1} = (\Phi_{p \times q})^- \ddot{y}_{p \times 1} \text{ (if } p = q) \end{cases} \quad (4)$$

in which $\hat{U}_{q \times 1}$ is the estimated modal acceleration responses. The error between the exact and estimated modal acceleration responses can be minimized by choosing the number of sensors to exceed the number of modes governing the responses of the super-tall building. In this study, the POD technique is employed to obtain the governing modes of a multi-degrees of freedom (MDOF) system (Chen and Kareem 2005, Azam and Marizani 2013). The energy contribution θ of the first q vibration modes can be determined based on the POD method

$$\theta = \frac{\sum_{i=1}^q \lambda_i}{\sum_{i=1}^n \lambda_i} \quad (1 \leq q \leq n) \quad (5)$$

where λ_i is the i th eigenvalue of the covariance matrix of the acceleration response, which represent the energy contribution to structural responses. The covariance matrix of the \ddot{y} is expressed as $R_{\ddot{y}} = E[\ddot{y} \ddot{y}^T]$. Generally, in order to obtain an accurate reduced-order representation of acceleration responses, the required energy contribution of the selected governing modes should exceed 99% of the total energy of the structural responses.

Substituting Eq. (2) into Eq. (1) and pre-multiplying each term in the ensuing equation by transposing the corresponding mode shape, Eq. (1) can be reduced to

$$M_i \ddot{U}_i + C_i \dot{U}_i + K_i U_i = \Phi_i^T F = f_i \quad (6)$$

where Φ_i is the i th mode shape. U_i and f_i are the modal displacement and modal wind load of the i th mode, respectively. M_i , C_i , and K_i are the modal mass, damping and stiffness of the i th mode, respectively.

If the mode shapes are mass orthonormal, that is

$$M_i = \Phi_i^T M \Phi_i = 1 \quad (i = 1, 2, \dots, n) \quad (7)$$

Eq. (6) can be rewritten in the state space as follows

$$\begin{bmatrix} \dot{U}_i \\ \ddot{U}_i \end{bmatrix} = \begin{bmatrix} 0 & 1 \\ -K_i & -C_i \end{bmatrix} \begin{bmatrix} U_i \\ \dot{U}_i \end{bmatrix} + \begin{bmatrix} 0 \\ 1 \end{bmatrix} f_i \quad (8)$$

Define

$$X_i(t) = [U_i \quad \dot{U}_i]^T \quad (9)$$

Table 1 The system matrices

	H_i	D_i
Acceleration	$[-K_i \quad -C_i]$	$[1]$
Displacement	$[1 \quad 0]$	$[0]$

Then, Eq. (8) becomes (Soong 1991)

$$\dot{X}_i(t) = A_i X_i(t) + B_i f_i \tag{10}$$

in which $A_i = \begin{bmatrix} 0 & 1 \\ -K_i & -C_i \end{bmatrix}$, $B_i = [0 \quad 1]^T$.

Based on Eq. (6), the measurement equation of the structural system can be written as

$$Z_i(t) = H_i X_i(t) + D_i f_i + \varepsilon_i \tag{11}$$

where $Z_i(t)$ represents the measured modal acceleration response. ε_i is the measurement noise vector in structural responses. The system matrices H_i and D_i are different, depending on the responses utilized (acceleration or displacement responses). These matrices are listed in Table 1.

Based on the continuous-time Kalman filter, the unmeasured displacement and velocity responses can be estimated by (Hwang *et al.* 2009, 2011)

$$\dot{\hat{X}}_i(t) = [A_i - G_i H_i] \hat{X}_i(t) + G_i Z_i(t) \tag{12}$$

where G_i denotes the Kalman filter gain matrix. $\hat{X}_i(t)$ denotes the estimated modal displacement and velocity of the i th mode.

Solving Eq. (12) yields

$$\hat{X}_i(t) = e^{[A_i - G_i H_i](t-t_0)} \hat{X}_i(t_0) + e^{[A_i - G_i H_i]t} \int_{t_0}^t e^{-[A_i - G_i H_i]\tau} G_i Z_i(\tau) d\tau \tag{13}$$

where $\hat{X}_i(t_0) = E[X_i(t_0)]$ is the initial modal displacement and velocity of the i th mode.

Since the measured acceleration responses are discrete time data, letting

$$t = m \cdot \Delta t \tag{14.1}$$

$$\tau = r \cdot \Delta t \tag{14.2}$$

Substituting the above equation into Eq. (13) yields

$$\begin{aligned} \hat{X}_i(m \cdot \Delta t) = & e^{[A_i - G_i H_i](m \cdot \Delta t - t_0)} \hat{X}_i(t_0) + \sum_{r=t_0/\Delta t}^m e^{[A_i - G_i H_i](m-r) \cdot \Delta t} G_i Z_i(r \cdot \Delta t) \Delta t - \\ & \frac{1}{2} e^{[A_i - G_i H_i](m \cdot \Delta t - t_0)} G_i Z_i(t_0) \Delta t - \frac{1}{2} G_i Z_i(m \cdot \Delta t) \Delta t \end{aligned} \tag{15}$$

in which Δ_t is the sampling interval for the observation vector $Z_i(t)$.

Table 2 The Riccati matrix \mathbf{P}_i

Response	Acceleration	Displacement
\mathbf{P}_i	$P_{11} = -(g^3 / K_i^2 + 2\mathbf{Q}_2^2 g / K_i - \mathbf{Q}_2 C_i g^2 / K_i^2) / (2\mathbf{Q}_2^2 K_i)$ $P_{12} = P_{21} = g^2 / (2\mathbf{Q}_2 K_i^2)$ $P_{22} = -g / K_i$	$P_{11} = \mathbf{Q}_2 \cdot g$ $P_{12} = P_{21} = \mathbf{Q}_2 \cdot g^2 / 2$ $P_{22} = -(\mathbf{Q}_2 g^4 / 4 - \mathbf{Q}_1 + K_i \mathbf{Q}_2 g^2) / (2C_i)$
g	$\mathbf{Q}_2 C_i - \sqrt{h - 2\mathbf{Q}_2^2 K_i + \mathbf{Q}_2^2 C_i^2}$	$\sqrt{h - 2K_i + C_i^2} - C_i$
h	$2K_i \cdot \sqrt{\mathbf{Q}_2^4 + \mathbf{Q}_1 \mathbf{Q}_2^3}$	$2 \cdot \sqrt{K_i^2 + \mathbf{Q}_1 / \mathbf{Q}_2}$

The Kalman filter gain in the above equations can be calculated by

$$\mathbf{G}_i = [\mathbf{B}_i \mathbf{Q}_1 \mathbf{D}_i^T + \mathbf{P}_i(t) \mathbf{H}_i^T] (\mathbf{D}_i \mathbf{Q}_1 \mathbf{D}_i^T + \mathbf{Q}_2)^{-1} \quad (16)$$

where \mathbf{Q}_1 and \mathbf{Q}_2 are the covariance matrices of the external load and noise, respectively. $\mathbf{P}_i(t)$ is the steady-state error covariance matrix and can be obtained by solving the following Riccati equation (Hwang *et al.* 2009, 2011)

$$\mathbf{A}_i \mathbf{P}_i(t) + \mathbf{P}_i(t) \mathbf{A}_i^T - [\mathbf{H}_i \mathbf{P}_i(t) + \mathbf{D}_i \mathbf{Q}_1 \mathbf{B}_i^T]^T (\mathbf{D}_i \mathbf{Q}_1 \mathbf{D}_i^T + \mathbf{Q}_2)^{-1} [\mathbf{H}_i \mathbf{P}_i(t) + \mathbf{D}_i \mathbf{Q}_1 \mathbf{B}_i^T] + \mathbf{B}_i \mathbf{Q}_1 \mathbf{B}_i^T = \mathbf{0} \quad (17)$$

Owing to the fact that \mathbf{Q}_1 and \mathbf{Q}_2 are unknown a priori, the following assumptions are adopted in this study for the wind load estimation of super-tall buildings

$$\mathbf{Q}_1 = E(\mathbf{f}\mathbf{f}^T) = \mathbf{I} \quad (18-1)$$

$$\mathbf{Q}_2 = E(\boldsymbol{\varepsilon}_i \boldsymbol{\varepsilon}_i^T) = \gamma \mathbf{I} \quad (18-2)$$

in which \mathbf{I} is an identity matrix, γ is an adjustment factor of noise.

Define

$$\mathbf{P}_i = \begin{bmatrix} P_{11} & P_{12} \\ P_{21} & P_{22} \end{bmatrix} \quad (19)$$

Substituting Eqs. (18) and (19) into Eq. (17) and solving the Riccati equation, the error covariance matrix can be determined. Listed in Table 2 are the element of matrix $\mathbf{P}_i(t)$ for different types of responses (acceleration or displacement responses). Finally, the Kalman filter gain can be calculated based on Eq. (16) and the matrix $\mathbf{P}_i(t)$, respectively.

It is noted that the observation vector $Z_i(t)$ represents the measured displacement response for the displacement feedback. Based on the corresponding matrices \mathbf{H}_i , \mathbf{D}_i and \mathbf{P}_i , the unknown responses can be estimated by using Eq. (12).

2.2 Estimation of wind load

In the previous section, the estimated wind-induced responses $\hat{\mathbf{X}}_i(t)$ of buildings can be calculated. Substituting $\hat{\mathbf{X}}_i(t)$ into Eq. (10) yields

$$\dot{\hat{\mathbf{X}}}_i(t) = \mathbf{A}_i \hat{\mathbf{X}}_i(t) + \mathbf{B}_i \hat{\mathbf{f}}_i \quad (20)$$

From Eq. (12), Eq. (20) can be rewritten as

$$\mathbf{B}_i \hat{\mathbf{f}}_i = \mathbf{G}_i [Z_i(t) - \mathbf{H}_i \hat{\mathbf{X}}_i(t)] \quad (21)$$

Using the pseudo-inverse \mathbf{B}_i^+ , Eq. (21) can be expressed as

$$\hat{\mathbf{f}}_i = \mathbf{B}_i^+ \mathbf{G}_i [Z_i(t) - \mathbf{H}_i \hat{\mathbf{X}}_i(t)] \quad (22)$$

Based on the inverse procedure described in the previous section, the first q modal wind loads $\hat{\mathbf{f}}_i (i=1,2,\dots,q)$ can be estimated from the corresponding decomposed modal responses, respectively.

Then, the estimated wind excitation time history vector can be calculated as

$$\hat{\mathbf{F}} = ((\Phi_{n \times q})^T)^+ \hat{\mathbf{f}} \quad (23)$$

where $\hat{\mathbf{f}}$ is the estimated modal load vector ($\hat{\mathbf{f}} = [\hat{f}_1 \ \hat{f}_2 \ \dots \ \hat{f}_q]^T$).

3. Wind load estimation for a super-tall building using wind tunnel test data

3.1 Experimental set-up

To verify the validity and accuracy of the proposed approach and investigate the characteristics of wind loads on super-tall buildings, the method is applied to estimate the wind loads on a super-tall building based on the wind tunnel test results. A proper comparison is also conducted between the wind loads determined by the present method and the wind tunnel test.

A super-tall building with a height of 371.7 m and 88 floors, located in the central district of Guangzhou, Guangdong Province, China is taken as an example structure herein. The site around the building can be regarded as terrain *C* (an urban area) according to the Chinese National Load Code (GB50009-2012). The general footprint of the building is approximately 45.8 m×45.8 m. The aspect ratio of the building's height to transverse width is about 8. Guangzhou is located in an active typhoon generating area of China. The concerned super-tall building may be subjected to severe wind forces induced by typhoons. All these facts made it necessary to investigate the performance of the super-tall building under strong wind conditions.

The Synchronous Multi-Pressure Scanning System (SMPSS) wind tunnel test for estimation of the wind effects on the super-tall building was carried out in the boundary wind tunnel at Shijiazhuang Tiedao University. The work section of the wind tunnel is approximately 24 m long, 4 m wide and 3 m high. According to the China Load Code (GB50009-2012), the exposure category *C* (corresponding to the exponent of the power law of mean speed profile of 0.22) are simulated at a length scale of 1/500 by setting spires, barriers, and rough elements in the test area. The measured mean wind profile and turbulence distribution are shown in Fig. 1. It can be found from the figure that the simulated wind profile of the fully developed boundary layer flow agrees with the power-law profile based on the parameters stipulated in the Chinese National Load Code, and the thickness of the simulated boundary layer is approximately 1 m. The turbulence intensity

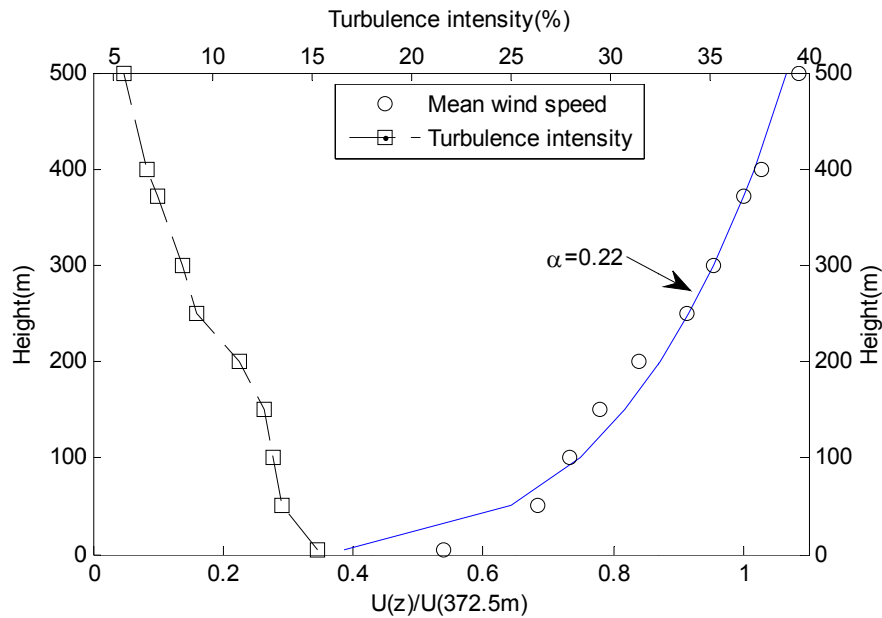


Fig. 1 Mean wind speed and turbulence intensity profiles



Fig. 2 Wind tunnel test model

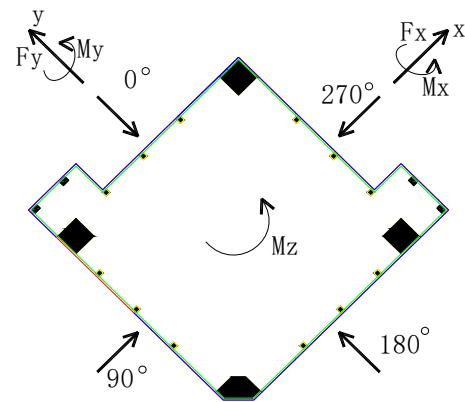


Fig. 3 Coordinate system

at the top of the model is almost 7.5%. The model has the same length scale with that of wind simulation, i.e., 1/500, representing a real building of a height of 371.7 m (see Fig. 2). In the wind tunnel tests, wind direction was defined as an angle β from the northwest along the anticlockwise direction varied from 0° to 360° with increments of 15° , as shown in Fig. 3. A total number of 441 pressure taps were installed on the building model for the pressure measurements. The pressure data were collected using four Scanivalve ZOC33 electronic pressure scanning modules, which were connected to a RAD3200 digital remote analog to the digital converter. The fluctuating wind pressure on the surfaces of the building model were continuously and simultaneously acquired and

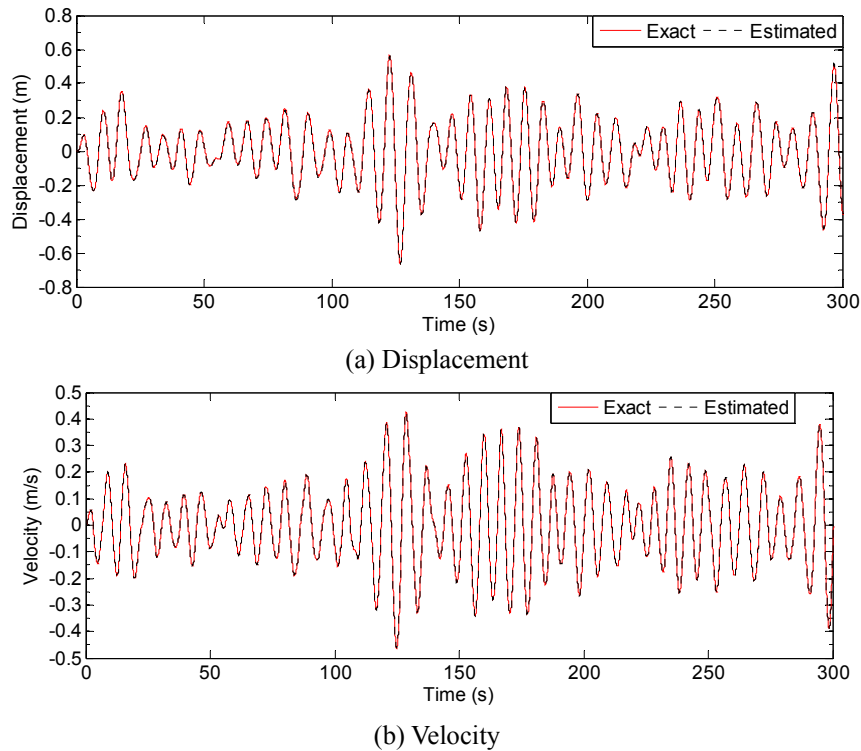


Fig. 4 Comparison of the time-histories of dynamic responses at the 80th floor in direction x under wind direction of 0°

digitized at 200 Hz. The wind speed at a height of 10m with a 100-year return period in Guangzhou is 30.5 m/s as specified in the China National Load Code (GB50009-2012). Based on the simultaneously measured pressures on the surfaces of the building model, time-histories of wind forces at each measurement layer with a 100-year return period were obtained. The measured wind forces, which are denoted as the exact wind loads in this paper, will be further compared with the estimated results obtained by the proposed inverse method in the next sections.

3.2 Wind load estimation

The wind-induced responses of the super-tall building cannot be determined directly from the SMPSS wind tunnel test. Hence, a direct dynamic analysis is conducted to obtain the wind-induced responses of the super-tall building. The system matrices (mass and stiffness) of the super-tall building can be established based on the finite element model. The damping matrix C of the structure can be determined by the Rayleigh damping model (Clough and Penzien 1993), where it was assumed to be proportional to the mass and stiffness matrices of the structural system. The damping ratio of the building is assumed to be 5%. The time-histories of the wind forces determined from the wind tunnel test were directly loaded onto the dynamic analysis model of the super-tall building. Then, the wind-induced dynamic responses (such as displacement, velocity and acceleration responses) can be calculated based on the wind tunnel test data and dynamic properties of the building. The obtained wind-induced response data will be used as the

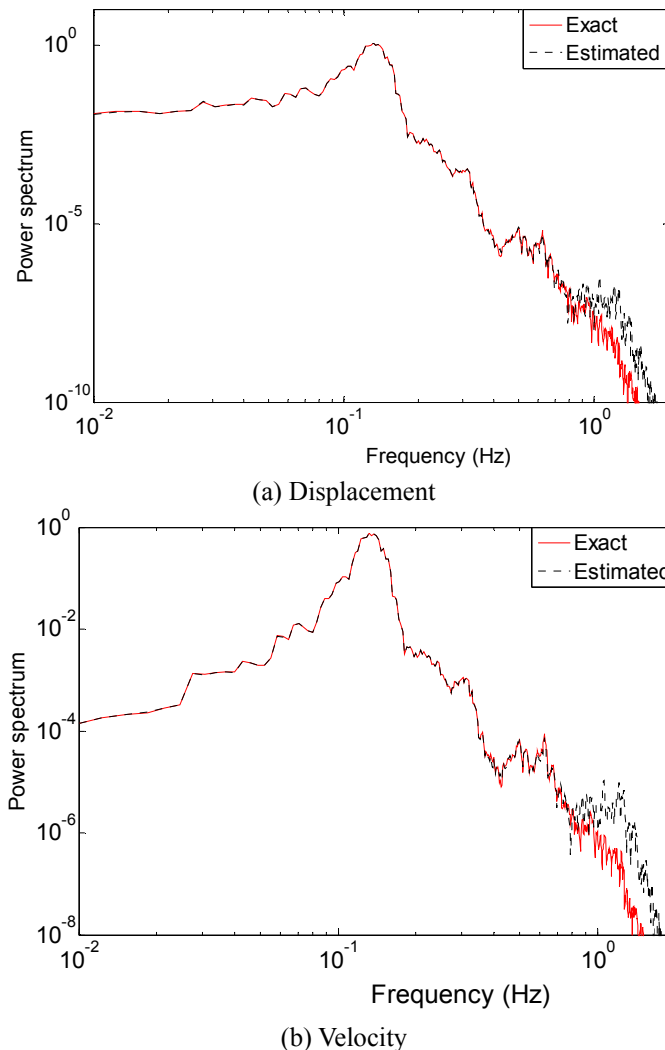


Fig. 5 Comparison of the PSD of dynamic responses at the 80th floor in direction x under wind direction of 0°

“measurement” data in the inverse analysis.

The wind loads are estimated by using the acceleration feedback in this section. The accelerations, which are induced by the fluctuating wind force components acting on a building, usually represent fluctuating components of wind-induced responses. As a result, only the fluctuating wind loads on the super-tall building are identified based on the selected wind-induced acceleration responses. By using Eq. (5), the vibration mode's energy contribution θ of the building can be calculated. The made observations indicate that the energy contribution of the first seven modes is over 99.6%. Therefore, the number of modes considered in this study is seven. Table 3 lists the first seven natural frequencies of the building. The calculated time-histories of acceleration responses at floors 25, 35, 50, 60, 70, 84 and 88 are adopted in the further investigation.

Based on the selected acceleration responses at the seven floors, the dynamic responses at the

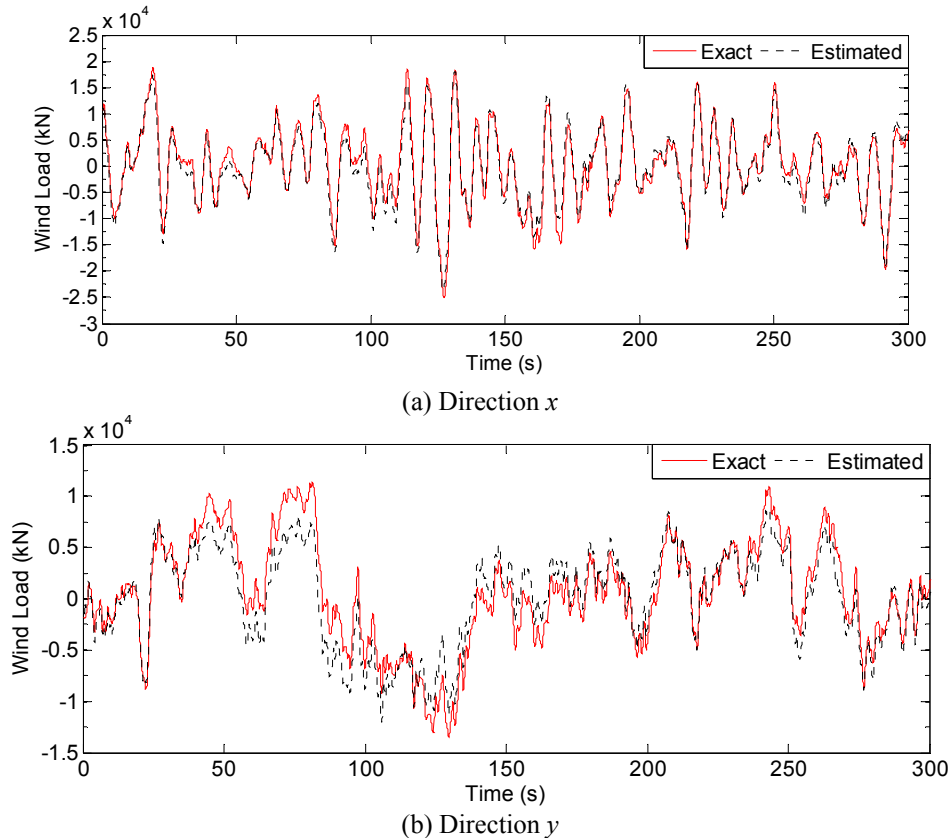


Fig. 6 Comparison of the time-histories of the total wind loads on the super-tall building under wind direction of 0°

other floors can be estimated by the presented scheme (Assuming $\gamma=10^{-8}$). Displayed in Fig. 4 is the comparison between the time histories of the identified wind-induced responses and the corresponding exact dynamic responses from computation based on the wind tunnel test results. It is observed that the estimated displacement and velocity responses agree well with the exact dynamic responses. Meanwhile, the power spectral density (PSD) of the estimated wind-induced responses obtained by the inverse method is presented in Fig. 5. The PSDs of the estimated responses are found to agree fairly well with those of the exact responses except slight differences in high frequency components ($>1\text{Hz}$). The main reason for these discrepancies may be attributed to that the higher-mode contributions ($>1\text{Hz}$) on the wind-induced responses of the super-tall building are neglect (see Table 3). Therefore, the proposed algorithm is applied successfully in the dynamic response estimation of super-tall structural systems in comparison with exact wind-induced responses. Furthermore, an obvious peak occurs at 0.138 Hz as shown in Fig. 5. This peak actually corresponds to the first translational natural frequency of the building in the x direction.

The wind loads acting on the super-tall building are identified by using the inverse algorithm described in Eqs. (20) to (23). Fig. 6 shows the time-histories of the estimated and the exact total wind loads in both x (across wind direction) and y (along wind direction) directions under the wind

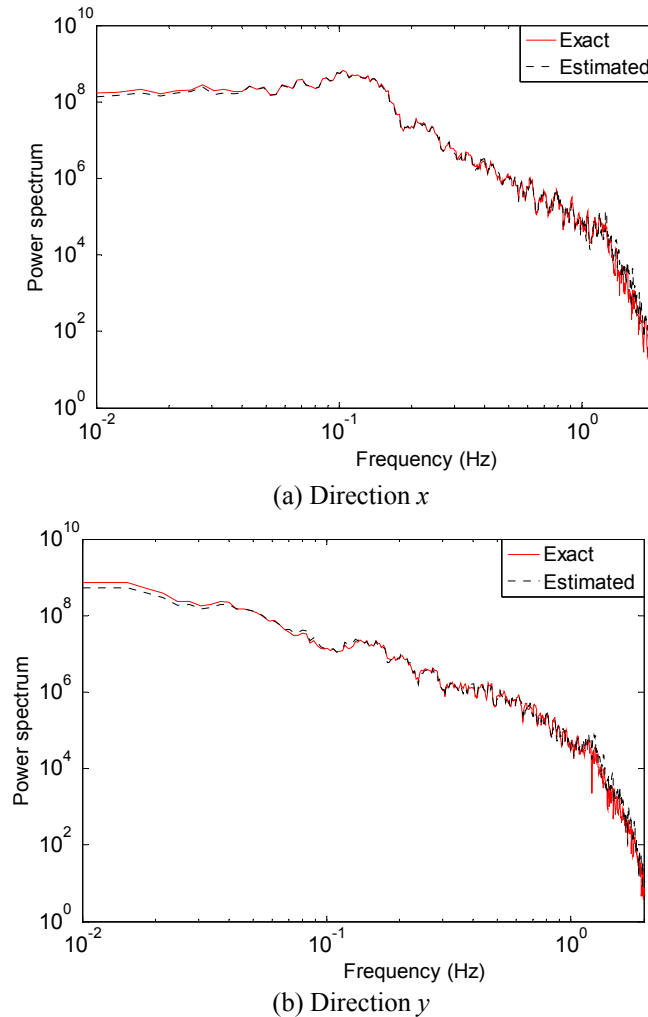


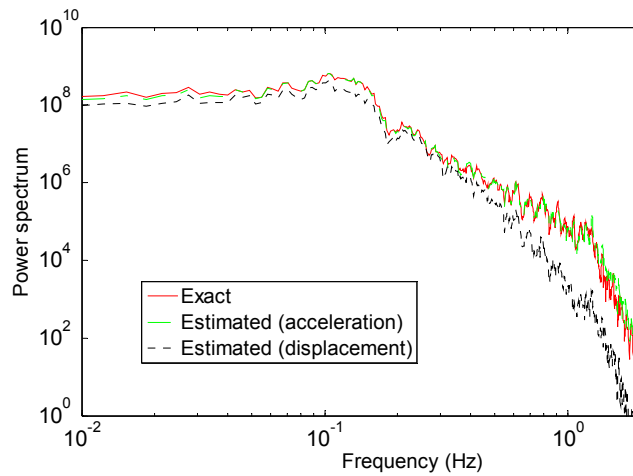
Fig. 7 Comparison of the PSD of the total wind forces on the super-tall building under wind direction of 0°

direction of 0° . The total wind loads on the building are calculated by integrating the wind loads on the 88 measurement layers (corresponding to the 88 floors of the building). It can be observed from the figure that the estimated wind loads in both directions are actually in good agreement with the exact ones. Furthermore, the wind force spectra in x and y directions obtained by the presented method are also displayed in Fig. 7. The estimated wind force spectra agree well with the exact spectra in both two directions in the whole frequency range. The analytical results indicate that the estimated wind force spectrum in the x direction (across-wind direction) has the main characteristics of a vortex-induced force spectrum, showing a sharp peak. The spectrum of the estimated wind force in the y direction (along-wind direction) is a typical longitudinal turbulence spectrum with a wide band. Table 4 shows the Root Mean Square (RMS) values of the estimated and exact wind loads in both x and y directions, which displays about -15.4 to -1.1% differences between the two sets of the results. The comparison demonstrates that the inverse method presented in this study is applicable to the engineering practice.

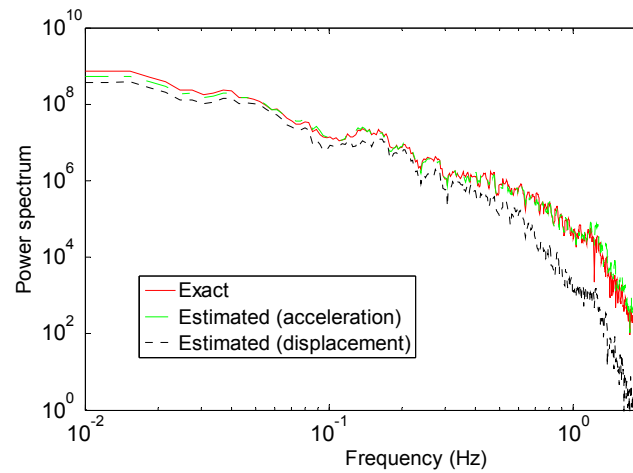
Table 4 The RMS values of the estimated and exact wind loads (kN)

Direction	<i>x</i>				<i>y</i>			
Wind direction	0°	90°	180°	270°	0°	90°	180°	270°
Estimated	7233	5364	7417	3783	4591	4765	4495	5456
Exact	7382	6339	7687	4300	5101	4.926	5225	5398
*Difference	-2.0%	-15.4%	-3.5%	-12.0%	-10.0%	-3.3%	-14.0%	1.1%

* Difference = (Estimated-Exact)/Exact.



(a) Direction *x*



(b) Direction *y*

Fig. 8 PSD of the estimated total wind forces on the super-tall building based on different response types under wind direction of 0°

3.3 Sensitivity to the type of wind-induced responses

The effects of the type of the wind-induced response on the wind load estimation are also

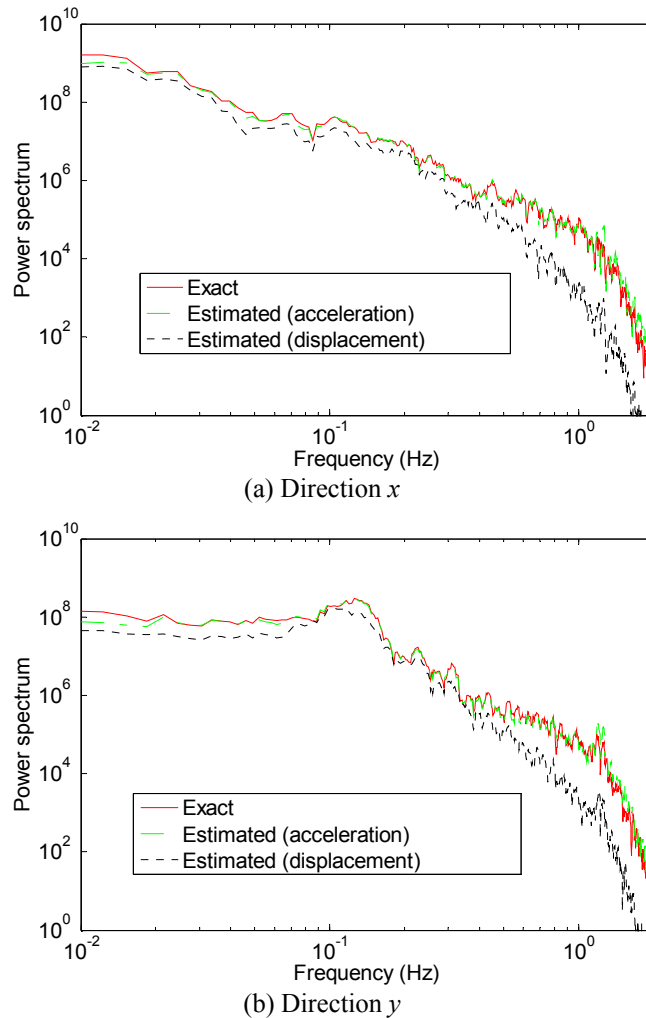


Fig. 9 PSD of the estimated total wind forces on the super-tall building based on different response types under wind direction of 90°

investigated based on the displacement and acceleration responses of the super-tall building in this study.

Displayed in Fig. 8 is the estimated and exact total wind force spectra in both x and y directions under the wind direction of 0° based on the displacement and acceleration responses, respectively. It is observed that the PSD curves of the estimated wind force spectra in two directions based on the acceleration feedback agree well with exact ones. However, the amplitudes of the estimated wind force spectra in both directions based on displacement responses are slightly smaller than that of the exact wind force spectra in the whole frequency range. Meanwhile, the estimated wind force spectra under 90° direction based on displacement and acceleration responses also presents the same tendency as shown in Fig. 9. The observations indicate that the acceleration feedback is more accurate in estimating wind loads than displacement response components, and the estimated results show limited dependency on the approaching wind direction.

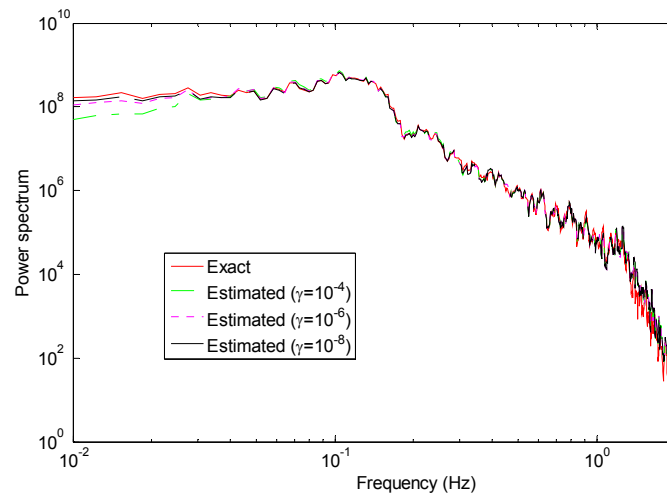
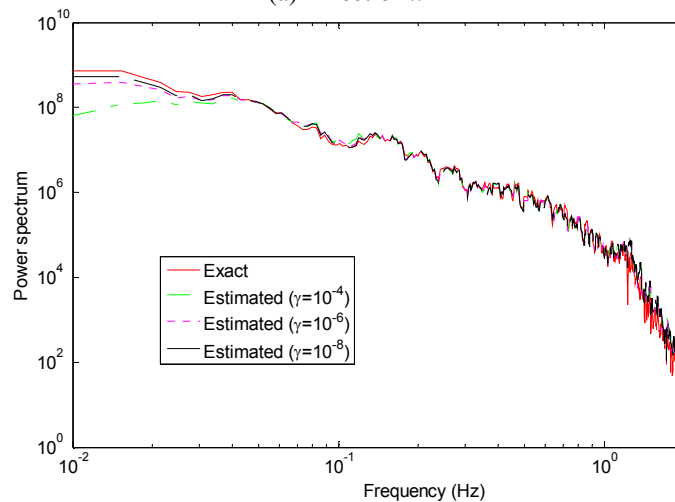
(a) Direction x (b) Direction y

Fig. 10 PSD of the estimated total wind forces on the super-tall building with different γ under wind direction of 0°

3.4 Effect of covariance matrix of noise

To examine effects of the covariance matrix of noise \mathbf{Q}_2 , the wind loads on the super-tall building are estimated with different γ . The PSD of the estimated total wind forces in both x and y directions under 0° direction are analyzed and displayed in Fig. 10 based on acceleration responses. For the purposes of comparison, the corresponding exact wind force spectra are also plotted in the figure. It is obvious that the amplitudes of the estimated total wind force spectra in the low frequency range simultaneously decreased with the increasing γ . However, less influence can be observed in the estimated wind force spectra in high frequency range. As illustrated in Fig. 10, one can find that variations of γ may induce effects on the algorithm performance to some extent. Satisfactory estimation efficacy can be achieved if the γ is in the range of 10^{-8} to 10^{-6} .

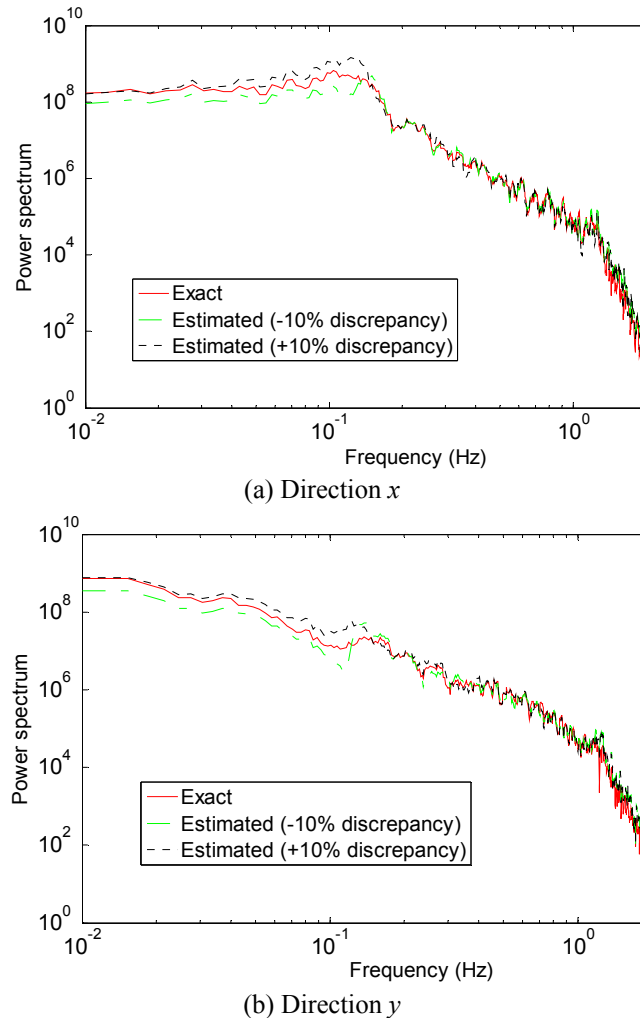


Fig. 11 The PSD of the total wind loads on the super-tall building for $\pm 10\%$ errors in natural frequency under wind direction of 0°

3.5 Effect of structural modal parameter error

Previous studies (Li *et al.* 2011, 2014, Zhi *et al.* 2011) illustrates that there were notable discrepancies between the theoretical dynamic characteristics predicted by the FEM and those from field measurements. In addition, structural modal parameters from field testing are often identified with uncertainty, which may induce some effects on the estimation of wind loads. In this study, the errors in modal parameters are set to be $\pm 10\%$. Fig. 11 shows the PSD of the estimated total wind loads on the super-tall building with $\pm 10\%$ errors in natural frequencies under 0° wind direction based on acceleration responses. For comparison purposes, the corresponding exact wind force spectra are also plotted in the figure. It can be observed that the spectra of estimated loads are slightly different from those of exact loads in the low-frequency range, which is applicable in engineering practice. Fig. 12 compared the estimated total wind loads on the building with the

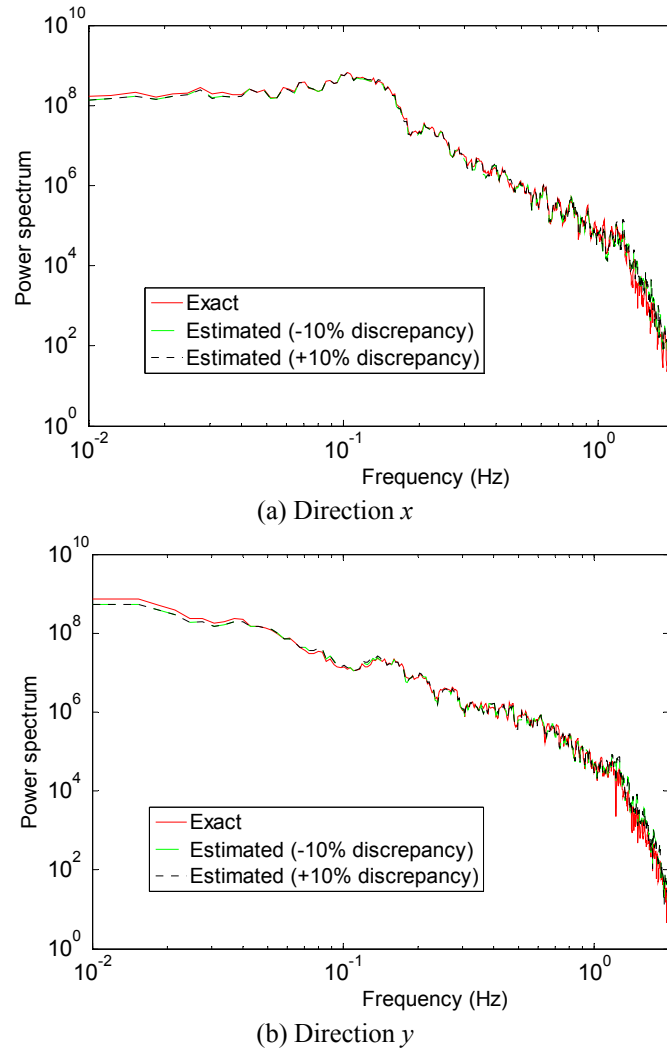


Fig. 12 The PSD of the total wind loads on the super-tall building for $\pm 10\%$ errors in damping ratio under wind direction of 0°

exact wind loads in the frequency domain with $\pm 10\%$ errors in damping ratios. It is seen that the estimated wind force spectra in both directions are very close to the exact wind force spectra. This implies that the identified results by the inverse method are not sensitive to the errors of modal parameters.

3.6 Effect of noise on the identification

Noise involved in measured signals is inevitable in actual applications. In order to examine the effects of the measurement noise on the identified quality, the artificial noise which is scaled with respect to the magnitude of the responses is superimposed on the exact responses. The acceleration feedback is employed for the inverse identification. Two noise levels of which the maximum

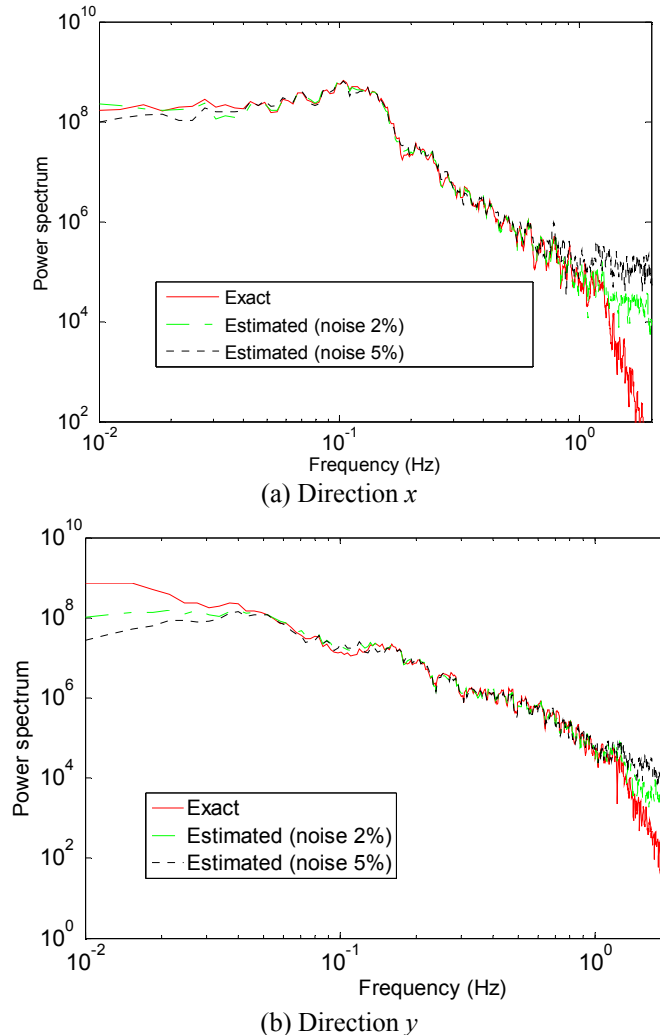


Fig. 13 The PSD of the total wind loads on the super-tall building with different noise levels under wind direction of 0°

values are scaled to be 2% and 5% of the maximum acceleration response are considered. Fig. 13 shows the comparison between the exact wind force spectra and the estimated wind force spectra for the different levels of noise, respectively. It is seen that the spectral density curves of the estimated wind forces are in good agreement with those of the exact wind forces in the concerned frequency range. However, some differences between the exact wind force spectra and the estimated wind force spectra can also be observed in the low and high frequency range. In order to eliminate the effects of the noise on the identification process, the estimated results for the case of 5% noise level are band-filtered and shown in Fig. 14. It can be observed that the quality of the estimated wind force spectrum is remarkably improved than before. The high frequency components in the identified wind load are eliminated with the aids of the signal filtering, which indicates that the band-pass filter may be a beneficial approach to improve the estimation efficacy.

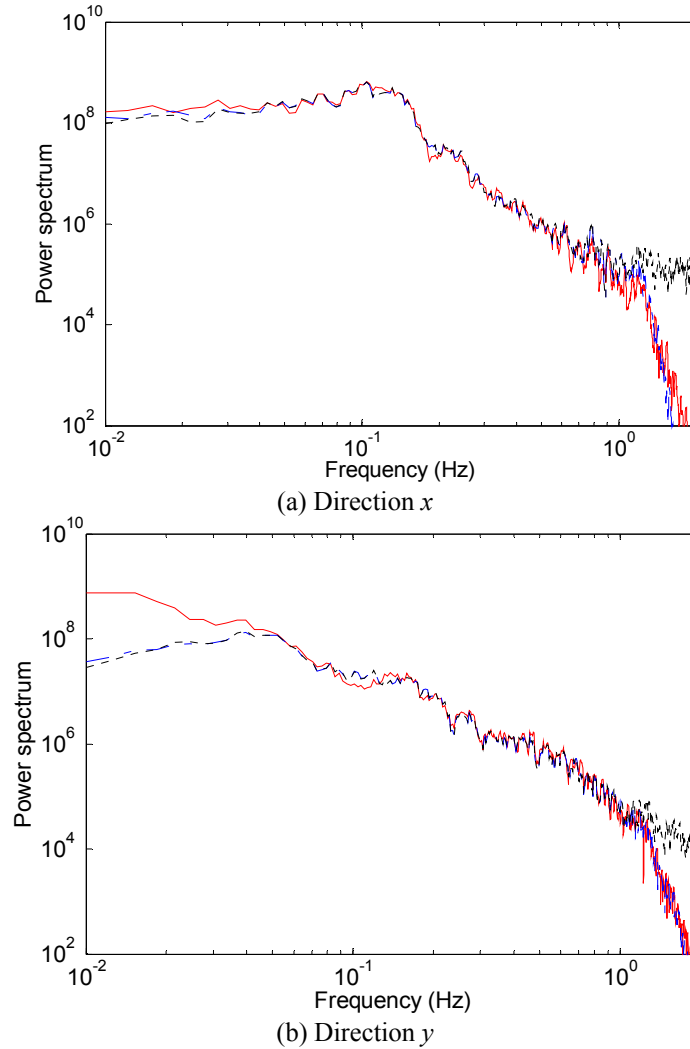


Fig. 14 The PSD of the estimated total wind loads on the super-tall building before and after the filtering operation under wind direction of 0° (Noise level=5%, — Exact, - - - - Estimated, - - - - Estimated after the filtering operation)

It is reported in literature that several alternative Kalman filtering-based methods have been proposed to identify external loads (Ma *et al.* 2003, Lourens *et al.* 2012, Naets *et al.* 2015). In order to assess the performances of the inverse method presented in this paper and the existing methods, a discrete Kalman filtering (DKF) based technique proposed by Lourens *et al.* (2012) is used to estimate the wind loads acting on the tall building, and compared to those obtained using the method developed in this study. Figs. 15 and 16 indicate the correlograms between the exact wind loads and the estimated ones for the DKF technique and the approach proposed in this paper, respectively, when 2% and 5% noise levels are include in the exact responses. The correlograms in these figures are obtained using the acceleration feedback. It is seen that the correlation coefficient

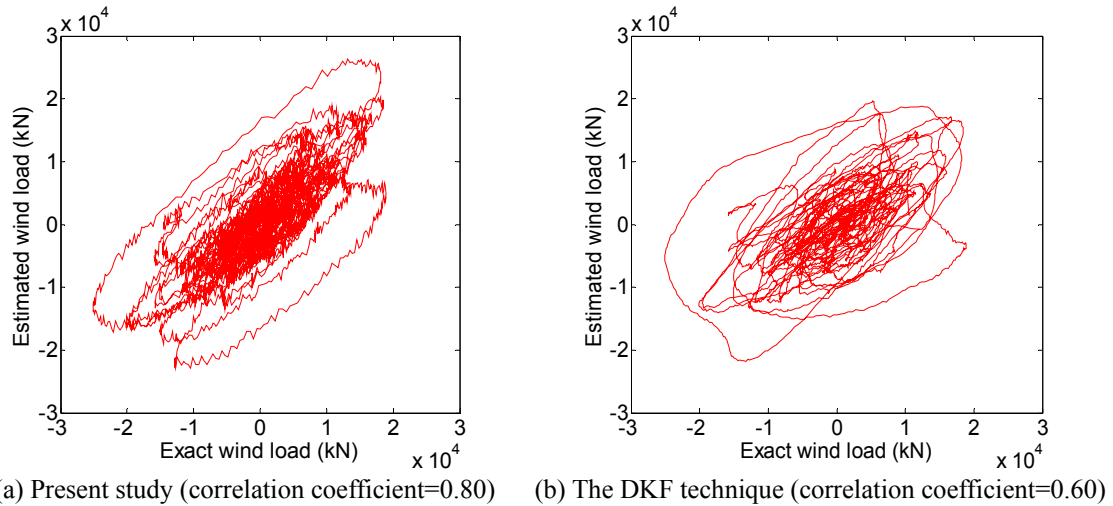


Fig. 15 Correlogram between the exact and estimated wind loads in direction x under wind direction of 0° (Noise level=2%)

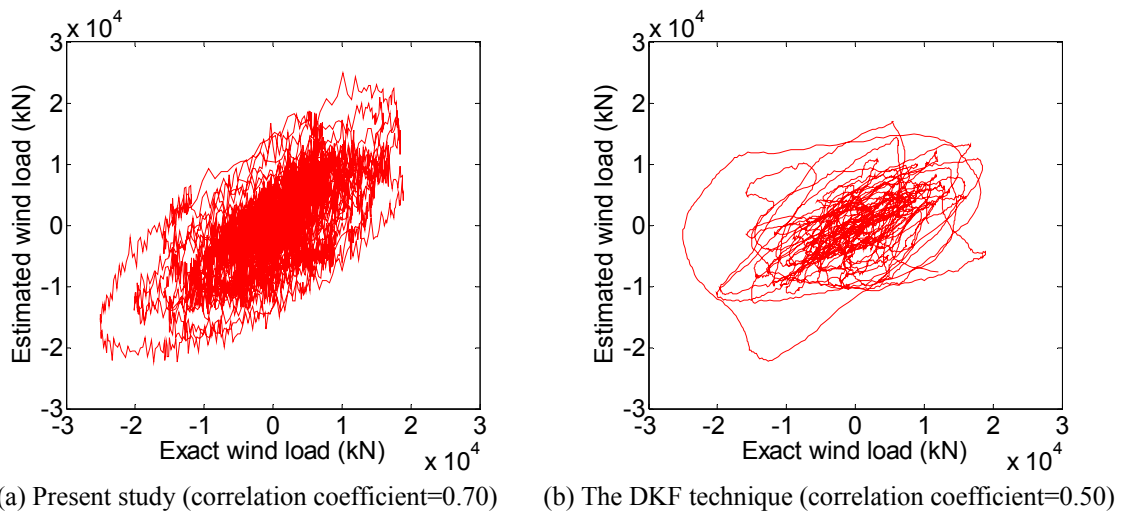


Fig. 16 Correlogram between the exact and estimated wind loads in direction x under wind direction of 0° (Noise level=5%)

by using two methods decreases as the noise level increases. The made observations also demonstrate that the correlation coefficients using the proposed method for two different noise levels are greater than those obtained from the DKF technique. Therefore, the rebuilt wind loads on the tall building by using the proposed approach is better than those based on the DKF method.

3.7 Effect of the number of vibration modes on the identification

To check the effects of the selected number of vibration modes on the identified wind loads, acceleration responses are used to identify the wind loads on the super-tall building with different

Table 5 The RMS values of the estimated wind loads from different number of modes (kN)

Direction	<i>x</i>			<i>y</i>		
	1 mode	3 modes	7 modes	1 mode	3 modes	7 modes
Total number of modes	1 mode	3 modes	7 modes	1 mode	3 modes	7 modes
Estimated	5683.6	7219.1	7232.6	4286.0	4658.1	4590.8
Exact	7381.6	7381.6	7381.6	5101.3	5101.3	5101.3
*Difference	-23%	-2.2%	-2%	-16%	-8.7%	-10%

*Difference= (Estimated-Exact)/Exact.

number of modes. Table 5 shows the RMS values of the estimated wind loads from different groups of vibration modes in two directions under 0° wind direction. It is observed that the higher mode contributions have considerable influence on the wind load estimation. Ignoring contribution of higher modes may lead to underestimation of wind loads. The estimation of across-wind forces (Direction *x*) is more sensitive to the considered number of vibration modes than those of along-wind forces (Direction *y*). There is no significant improvement in the identified quality when the mode number is more than three. This observation indicates that the wind load estimation for super-tall structures with uniform mass and stiffness distributions along the building height can be accurately assessed by the first three vibration modes.

4. Conclusions

An inverse method to estimate wind loads on super-tall buildings using limited measurement responses is actively developed and investigated based on the continuous-time Kalman filter in this study. The optimum Kalman filter gain is determined for different types of wind-induced responses by solving the Riccati equation. The estimation quality of the proposed approach is evaluated through a SMPSS wind tunnel test of an example super-tall building.

The verification and validation observations indicate that the estimated wind-induced responses agree well with the exact responses. The estimated and exact wind loads on the super-tall building in the time and frequency domains are in good agreement. The difference of the RMS wind loads between the estimated and exact results under different wind directions is very small, which implies that the proposed algorithm can be applied in practice.

The experimental results also demonstrate that the acceleration feedback is more accurate in estimating the wind loads than the displacement feedback. The estimation performance of the proposed algorithm is affected by variations of γ . The results implied that γ values of 10^{-8} - 10^{-6} appear reasonable for the wind load estimation of super-tall buildings. The estimation of the wind forces for super-tall buildings is insensitive to errors of modal parameters. The identified results indicated that the efficiency of the developed method decreased with the increasing noise intensity and can be improved by a band-pass filter. The estimated wind loads using the proposed approach under different noise levels are more accurate than those by the DKF approach. Furthermore, the dependency of identification with the number of vibration modes of the super-tall building cannot be negligible. Therefore, it is concluded that the developed inverse method is an effective tool for predicting the wind loads on super-tall buildings.

Acknowledgements

The work described in this paper was fully supported by grants from the National Natural Science Foundation of China (Project No: 51208404 and 51478371) and a grant from the Fok Ying Tong Education Foundation, China (Project No: 141074).

Reference

- Azam, S.E. and Mariani, S. (2013), "Investigation of computational and accuracy issues in POD-based reduced order modeling of dynamic structural systems", *Eng. Struct.*, **54**, 150-167.
- Azam, S.E., Chatzi, E. and Papadimitriou, C. (2015), "A dual Kalman filter approach for state estimation via output-only acceleration measurements", *Mech. Syst. Signal Pr.*, **60**, 866-886.
- Chakraborty, S., Dalui, S.K. and Ahuja, A.K. (2014), "Wind load on irregular plan shaped tall building-a case study", *Wind Struct.*, **19**(1), 59-73.
- Chen, J. and Li, J. (2001), "Study on wind load inverse of tall building", *Chin. Quart. Mech.*, **22**(1), 72-77. (in Chinese)
- Chen, X.Z. and Kareem, A. (2005), "Proper orthogonal decomposition-based modeling, analysis, and simulation of dynamic wind load effects on structures", *J. Eng. Mech.*, ASCE, **131**(4), 325-339.
- Clough, R.W. and Penzien, J. (1993), *Dynamics of Structures*, 2nd Edition, McGraw-Hill, Inc., New York.
- Council on tall buildings and urban habitat (2015), CTBUH Height Criteria. <<http://www.ctbuh.org/HighRiseInfo/TallestDatabase/Criteria/tabid/446/language/en-US/Default.aspx>>.
- GB50009-2012 (2012), *Load code for the design of building structures*, China Architecture & Building Press, Beijing.
- Ha, Y.C. (2013), "Empirical formulations for evaluation of across-wind dynamic loads on rectangular tall buildings", *Wind Struct.*, **16**(6), 603-616.
- Hwang, J.S., Kareem, A. and Kim, H.J. (2009), "Estimation of modal loads using structural response", *J. Sound Vib.*, **326**, 522-539.
- Hwang, J.S., Kareem, A. and Kim, H.J. (2011), "Wind load identification using wind tunnel test data by inverse analysis", *J. Wind Eng. Indus. Aerodyn.*, **99**(1), 18-26.
- Kalman, R.E. and Bucy, R.S. (1961), "New results in linear filtering and prediction theory", *Am. Soc. Mech. Eng. J. Basic Eng.*, **83**(3), 95-108.
- Kang, C.C. and Lo, C.Y. (2002), "An inverse vibration analysis of a tower subjected to wind drags on a shaking ground", *Appl. Math. Model.*, **26**, 517-528.
- Law, S.S., Bu, J.Q. and Zhu, X.Q. (2005), "Time-varying wind load identification from structural responses", *Eng. Struct.*, **27**, 1586-1598.
- Li, Q.S., Zhi, L.H., Tuan, A.Y., Kao, S.H., Su, S.C. and Wu, C.F. (2011), "Dynamic behavior of Taipei 101 Tower: field measurement and numerical analysis", *J. Struct. Eng.*, ASCE, **137**(1), 143-155.
- Li, Q.S., Zhi, L.H., Yi, J., To, A. and Xie, J.M. (2014), "Monitoring of typhoon effects on a super-tall building in Hong Kong", *Struct. Control Health Monit.*, **21**(6), 926-949.
- Lourens, E., Papadimitriou, C., Gillijns, S., Reynders, E., De Roeck, G. and Lombaert, G. (2012), "Joint input-response estimation for structural systems based on reduced-order models and vibration data from a limited number of sensors", *Mech. Syst. Signal Pr.*, **29**, 310-327.
- Ma, C.K., Chang, J.M. and Lin, D.C. (2003), "Input forces estimation of beam structures by an inverse method", *J. Sound Vib.*, **259**(2), 387-407.
- Nagashima, I., Maseki, R., Asami, Y., Hirai, J. and Abiru, H. (2001), "Performance of hybrid mass damper system applied to a 36-storey high-rise building", *Earthq. Eng. Struct. Dyn.*, **30**, 1615-1637.
- Naets, F., Cuadrado, J. and Desmet, W. (2015), "Stable force identification in structural dynamics using Kalman filtering and dummy-measurements", *Mech. Syst. Signal Pr.*, **5051**, 235-248.
- Sanchez, J. and Benaroya, H. (2014), "Review of force reconstruction techniques", *J. Sound Vib.*, **33**,

2999-3018.

Soong, T.T. (1991), *Active Structural Control: Theory and Practice*, Longman, New York, USA.

Stevens, K.K. (1987), "Force identification problems-an overview", *Proceedings of the 1987 SEM Spring Conference on Experimental Mechanics*, Houston, June.

Zhi, L.H., Li, Q.S., Wu, J.R. and Li, Z.N. (2011), "Field monitoring of wind effects on a super-tall building during typhoons", *Wind Struct.*, **14**(3), 1-31.

Wu, S.Q. and Law, S.S. (2010), "Moving force identification based on stochastic finite element model", *Eng. Struct.*, **32**, 1016-1027.

CC

Nomenclature

A_i	2×2 dimensional system matrix of the i -th mode
B_i	2×1 dimensional system matrix of the i -th mode
C	$n \times n$ dimensional damping matrix
C_i	i -th modal damping coefficient
E	expectation sign
f_i	i -th modal wind load
F	n -dimensional wind force vector
G_i	Kalman filter gain matrix
H_i	observation matrix
I	identity matrix
K	$n \times n$ dimensional stiffness matrix
K_i	i -th modal stiffness
M	$n \times n$ dimensional mass matrix
M_i	i -th modal mass
n	degree of freedom of structure
p	number of sensors
$P_i(t)$	covariance matrix of error
q	number of identified mode shapes
Q_1	covariance matrix of external load
Q_2	covariance matrix of noise
U_i	i -th modal displacement
$\ddot{U}_{n \times 1}$	n -dimensional modal acceleration response
$\ddot{U}_{q \times 1}$	q -dimensional modal acceleration
$\hat{\ddot{U}}_{q \times 1}$	q -dimensional estimated acceleration responses in modal space
$X_i(t)$	i -th modal state variable
$\hat{X}_i(t)$	i -th estimated state variable in modal space
y	n -dimensional displacement vector
\dot{y}	n -dimensional velocity vector
\ddot{y}	n -dimensional acceleration vector
$\ddot{y}_{p \times 1}$	p -dimensional vector of measured acceleration

$\mathbf{Z}_i(t)$	measured modal response
γ	adjustment factor of noise
ε_i	measurement noise vector in structural response
λ_i	i -th eigenvalue of covariance matrix of responses
θ	energy contribution of the first q vibration modes
Δt	sampling interval for observation vector
$\Phi_{n \times n}$	$n \times n$ mode shape matrix
$\Phi_{p \times q}$	$p \times q$ mode shape matrix
$\Phi_{n \times n}^+$	generalized inverse of matrix $\Phi_{n \times n}$
$\Phi_{n \times n}^-$	inverse of matrix $\Phi_{n \times n}$
Φ_i	i -th mode shape